Reliability of Capacitive RF MEMS Switches at High and Low Temperatures

Yong Zhu, Horacio D. Espinosa

Department of Mechanical Engineering, Northwestern University, 2145 Sheridan Rd., Evanston, IL 60208-3111

Received 1 September 2003; accepted 24 February 2003

ABSTRACT: Some applications of RF MEMS switches, such as aircraft condition monitoring and distributed satellite communication, present a unique challenge for device design and reliability. This article examines these switches when operational temperatures in the range −60°C to 100°C are envisioned. The basic operation of a capacitive MEMS switch is described and two tools for examining device reliability, modeling, and on-chip experimentation, are discussed in the case of capacitive MEMS switches. 1D, 2D, and 3D models are presented with emphasis on 3D coupled-field finite-element analysis, including temperature effects. Results and findings from the 3D simulations are reported. In particular, the advantages of employing corrugated membranes in the design of RF MEMS switches are assessed. Their performance in terms of reliability as a function of temperature is quantified. The effects of corrugation on the geometric parameters are discussed in the context of device-design optimization. In order to assess reliability experimentally, the M-test and the membrane deflection experiment (MDE) are reviewed due to their on-chip characteristic and simplicity. Ways in which these experimental/computational methodologies can be combined for identifying material properties and device performance is also highlighted. © 2004 Wiley Periodicals, Inc. Int J RF and Microwave CAE 14: 317–328, 2004.

Keywords: MEMS; RF switch, reliability; mechanical testing; MEMS modeling; coupled analysis

I. INTRODUCTION

Microelectromechanical systems (MEMS) technology enables batch fabrication of miniature mechanical transducers integrated with complementary metal-oxide semiconductor (CMOS) circuits. The increasing demand for more flexible and functional, yet lightweight and low-power-consumption wireless systems, has generated the need for a technology that can dramatically reduce manufacturing cost, size, and weight, and improve performance and reliability. MEMS for radio frequency (RF) applications, called RF MEMS, provides an opportunity to meet these requirements.

Correspondence to: H. D. Espinosa; email: espinosa@northwestern.edu.

Published online in Wiley InterScience (www.interscience.wiley.com). DOI 10.1002/mmce.20015

Reliability of MEMS components is of major concern for long-term and broad-based applications, and it is currently an area of intense research [1]. For capacitive MEMS switches, the major reliability problem is stiction between the metal layer (top electrode) and the dielectric layer covering the bottom electrode. The failure is believed to be result of charge build-up in the dielectric material. This charge build-up is strictly related to the actuation voltage [2]. A reduction in the actuation voltage by 6 V results in a tenfold increase in the lifetime of typical MEMS switches. The actuation voltage is usually related to the device geometry, mechanical properties, and residual stress state. Electromechanical analysis and on-chip experimentation are vital for improved design of these devices.

Some applications of RF MEMS switches, such as aircraft-condition monitoring and distributed-satellite

communication [3], require low operational temperature (for example, −60°C). By contrast, the temperature during device packaging can reach 200°C [4] and, as a result, affect the post-package device performance. Hence, device reliability as a function of temperature presents a major challenge for the designer of MEMS switches. It has been reported that a moderate temperature increase may cause buckling of the switch structure, which leads to a premature failure of the device. On the other hand, temperature reduction could result in a significant increase of the pull-in voltage, which is undesirable [5]. Therefore, it is relevant to design a switch with a structure and materials that are almost insensitive to temperature variations.

Investigation of the reliability of capacitive MEMS switches at high and low temperatures is the subject of this article. Electromechanical modeling, which accounts for thermally induced stresses, and experimental techniques suitable to this endeavor are discussed with emphasis on the usage of corrugated membranes as a candidate for stress relaxation within the structure. The article is organized as follows: (i) various models for electromechanical analysis of MEMS switches are presented and the applicability of each model is discussed, (ii) corrugated membranes are examined in detail in the context of reliability versus temperature using 3D coupled-field finite-element analysis (FEA) modeling, (iii) available on-chip experimentation techniques are reviewed for the purpose of reliability testing at various temperatures, and (iv) concluding remarks on the design of RF MEMS switches are summarized.

II. ELECTROMECHANICAL MODELING OF RF MEMS SWITCHES

A typical capacitive RF MEMS switch consists of a fixed-fixed thin metallic membrane which is suspended over a bottom electrode insulated by a dielectric film. When the switch is not actuated, there is low capacitance between the membrane and the bottom electrode, and the device is in the OFF state [6]. When voltage is applied between the movable structure and the fixed bottom electrode, electrostatic charges are induced on both the movable structure and the bottom electrode. The electrostatic charges cause a distributed electrostatic force, which deforms the movable structure. In turn, such deformation leads to storage of elastic energy, which tries to restore the structure to its original shape. The structure deformation also results in the reorganization of all surface charges on the device. This reorganization of charges causes further structural deformation; hence, the device exhibits a highly nonlinear, coupled electromechanical behavior. Until a certain voltage is applied, the so-called pull-in voltage or actuation voltage, an equilibrium position exists through a balance between the elastic restoring force and electrostatic force. After pull-in, the device is in the ON state and its capacitance is much larger than that in the OFF state.

The switch actuation is therefore a coupled-field problem of electrostatics and structural response. In order to accurately describe the switch deformation and predict the pull-in voltage, an effort to realize modeling has to be made. In the following section, we will discuss a simple 1D parallel-plate actuator model [7, 8], a 2D distributed model [9, 10], and a 3D fully coupled model [11, 12]. The analyses and simulations are dedicated to capacitive MEMS switches, although they are also applicable to other types of electrostatic devices.

2.1. 1D Parallel-Plate Actuator Model

A first-order approximation of this device is a system consisting of two parallel plates separated by gap g_0, with one plate fixed on the substrate and the other suspended by a linear spring [Fig. 1(a)]. When a voltage V is applied across the plates, the force balance equation is given by

$$\frac{\varepsilon A V^2}{2(g_0 - w)^2} - K_{eff} w = 0, \tag{1}$$

where $K_{eff} = (32Ebt^3)/L^3 + (8T)/L$ is the effective structural stiffness, $T = \sigma_0 (1 - v)bt$, A is the area of the movable plate, ε is the electric permittivity of free space, g_0 is the initial gap, w is the deflection, E is the Young's modulus, t is the plate thickness, σ_0 is the biaxial residual stress presumed present before the plate shape is etched, and v is the Poisson's ratio.

As V increases, the movable plate is deflected down gradually. However, at the pull-in voltage, $V_{pull\text{-}in} = \sqrt{(8k_{eff})/(27\varepsilon A)\, g_0^3}$, *the system becomes unstable and the plate suddenly collapses. The corresponding gap is* $2/3 g_0$.

This linear spring approximation works quite well for the small deflection regime of the switch membrane. Here small deflection means the deflection is comparably smaller than the membrane thickness. However, for a capacitive MEMS switches the deflection is usually tens of times larger than its thickness [6, 7]. Hence, to describe the switch membrane deflection, a Duffing spring with a nonlinear term can be used instead. Then the force balance equation becomes

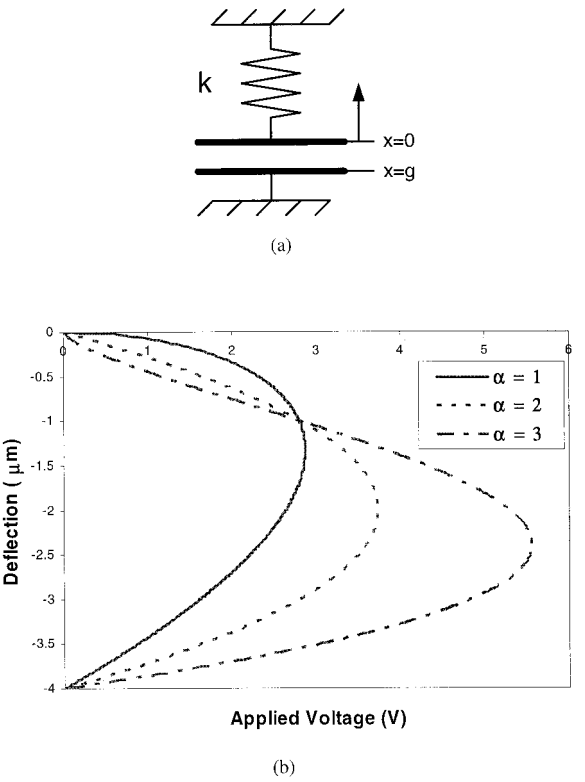

Figure 1. (a) Schematic of the 1D parallel-plate actuator model; (b) pull-in curves for the 1D model with the spring constitutive law given by $F_m = kw^\alpha$, where k is an arbitrary number.

$$\frac{\varepsilon A V^2}{2(g_0 - w)^2} - k_1 w - k_3 w^3 = 0, \tag{2}$$

where $K_1 = (32Ebt^3)/L^3 + (8T)/L^2$ and $k_3 = (\pi^4 Ebt)/(8L^3)$ [1]. The first order term in the Duffing spring arises from the switch membrane bending and residual stress, and the third order term originates from the strain stiffening effect. As the switch membrane deflects, the tensile stress in the membrane increases due to in-plane strain (a form of geometric nonlinearity). This tensile stress increases the membrane stiffness. At large deflection, the strain stiffening effect can become dominant.

Not only does the effect of strain stiffening increase the pull-in voltage, but also increases the deflection range before pull-in [8]. In general, the spring restoring force and the gap at pull-in instability are related as

$$F_m = kw^\alpha, \tag{3a}$$

$$g_{pull\text{-}in} = \frac{2}{2 + \alpha} g_0, \tag{3b}$$

where k and α are index factors representing the constitutive relation (for example, $\alpha = 1, 2, 3$).

When $\alpha = 1$ (at small deflection, where bending and residual stress are dominant), the gap at pull-in is 2/3 of the initial gap, which is the case of the linear spring parallel-plate actuator. By contrast, when $\alpha = 3$ (at large deflection, where the strain stiffening effect is dominant), the gap at pull-in is 2/5 of the initial gap. Figure 1(b) shows the pull-in curves corresponding to $\alpha = 1$, 2, and 3 respectively. In practice, the pull-in gap lies between $\frac{2}{3} g_0$ and $\frac{2}{5} g_0$, depending upon the device geometry and residual stress state.

As a matter of fact, Hung and Senturia took advantage of this large motion before pull-in instability to extend the travel range of electrostatic actuators [8]. Figure 1(b) also shows that when $\alpha = 3$, the deflection-applied voltage curve is concave up with a large range in applied voltage of nearly constant slope.

2.2. 2D Distributed Model

Since the deflection along the switch membrane is not uniform, the electrostatic field is accordingly position-dependent rather than uniform, as assumed in the 1D model. The 2D distributed model [9, 10] for a capacitive MEMS switch is based on beam theory. For a rectangular-shaped switch, since its width is comparable to its length, a cross section of the switch membrane is considered as the case of plane strain (see Fig. 2). Under distributed electrostatic force, the differential equation describing the plate deflection is given by

$$\tilde{E} I \frac{d^4 w}{dx^4} - T \frac{d^2 w}{dx^2} = -\frac{\varepsilon b V^2}{2(g_0 - w)^2}, \tag{4}$$

where $\tilde{E} = E/(1 - \nu^2)$ is the plate modulus, $I = \frac{1}{12} bt^3$ is the moment of inertia with respect to the neutral axis, and b is the plate width. The fringing field is neglected for the capacitive switch, since its gap is much smaller than its side length.

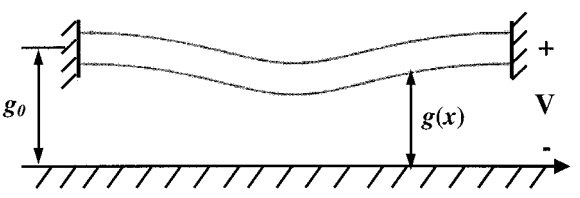

Figure 2. Schematic of 2D distributed model. Note that the switch membrane deflection is not uniform and that as a result the electrostatic force is therefore position dependent.

Eq. (4) is a linear distributed model and only valid for small deflections. At large deflections, again the strain stiffening effect has to be included. The von Karman plate equation considers this effect and is written as

$$\tilde{E}I\frac{d^4w}{dx^4} = -\frac{\varepsilon b V_0^2}{2(g_0 - w)^2} + \frac{Ebt}{2}\left(\frac{dw}{dx}\right)^2\left(\frac{d^2w}{dx^2}\right) + T\left(\frac{d^2w}{dx^2}\right), \quad (5)$$

where the first term on the right arises from the electrostatic force, the second term originates from nonlinear kinematics, and the third term derives from the residual stress. For a rectangular switch membrane, Eq. (5) can be easily integrated numerically and provides precise answers when compared to a 3D full simulation [11–12].

2.3. 3D Full Model

If the switch membrane is not rectangular or circular, it is inaccurate to assume plane strain and use 2D beam model. Rather, a 3D distributed plate model should be used. The partial differential equation (PDE) describing the plate deflection is given by

$$\nabla^4 w = \frac{1}{D}\left[\frac{\varepsilon V_0^2}{2(g_0 - w)^2} + \sigma_0 t\left(\frac{\partial^2 w}{\partial x^2}\right) + \sigma_0 t\left(\frac{\partial^2 w}{\partial y^2}\right)\right], \quad (6)$$

where $\nabla^4(\,) \equiv \partial^4/(\partial x^4) + \partial^4/(\partial x^2 \partial y^2) + \partial^4/(\partial y^4)$ $D = Et^3/12(1 - \nu^2)$ is flextual rigidity of the plate.

The in-plane strains due to large deflection are

$$\varepsilon_x = \frac{1}{2}\left[\frac{\partial w(x, y)}{\partial y}\right]^2 \quad (7a)$$

$$\varepsilon_y = \frac{1}{2}\left[\frac{\partial w(x, y)}{\partial x}\right]^2, \quad (7b)$$

$$\omega = \frac{\partial w(x, y)}{\partial x}\frac{\partial w(x, y)}{\partial y}, \quad (7c)$$

where ε_x and ε_y are normal strains and ω is shear strain. As a result, the large deflection is described by [13]

$$\nabla^4 w = \frac{1}{D}\left[\frac{\varepsilon V_0^2}{2(g_0 - w)^2} + Et(\varepsilon_x + \nu\varepsilon_y)\left(\frac{\partial^2 w}{\partial x^2}\right) + Et(\varepsilon_y + \nu\varepsilon_x)\left(\frac{\partial^2 w}{\partial y^2}\right) - Et(1 - \nu)\omega\left(\frac{\partial^2 w}{\partial x \partial y}\right) + \sigma_0 t\left(\left(\frac{\partial^2 w}{\partial x^2}\right) + \left(\frac{\partial^2 w}{\partial y^2}\right)\right)\right]. \quad (8)$$

This 3D plate model can describe the case of various in-plane shapes and even nonuniform residual stresses. Nevertheless, an out-of-plane profile is typically present in the MEMS switch. In addition, when operational temperature varies, the switch geometry and residual stress-state vary accordingly, which makes the problem even more complicated. In this case, a coupled-field finite-element analysis (FEA), including structural, electrostatic and thermal domains, is required.

2.4. 3D FEA Model

The numerical methods employed for coupled-field analysis have been based thus far on the relaxation method, the surface Newton method, and the tightly coupled Newton method. Corning Intellisense, Coventor, and MEMSCAP have developed integrated electromechanical software packages for these coupled-field problems [1]. Recently, the authors have implemented a 3D FEA model and simulated MEMS switches at various operational temperatures using ANSYS [11, 12]. The simulation consisted of two steps in sequence: a thermo-structural analysis followed by an electrostatic-structural analysis. If the temperature is constant, only the second step, electrostatic-structural analysis, is needed. Before the simulation, the solid model (consisting of the switch, the bottom electrode, and the surrounding medium), is constructed. Two physical environments—electrostatic and structural environments—are defined based on the solid-model and boundary conditions. Shell elements are employed to model the switch membrane and solid elements are used to model the surrounding medium to account for the electrostatic field. The material parameters of the membrane, Young's modulus, Poisson ratio, and thermal-expansion coefficient, are assigned to the shell elements and that of the surrounding medium, electric permittivity, is assigned to the solid elements. Iterations between these two physical environments are executed in sequence until convergence in both environments is reached. This process is repeated for every applied voltage. The pull-in voltage is identified when a convergent solu-

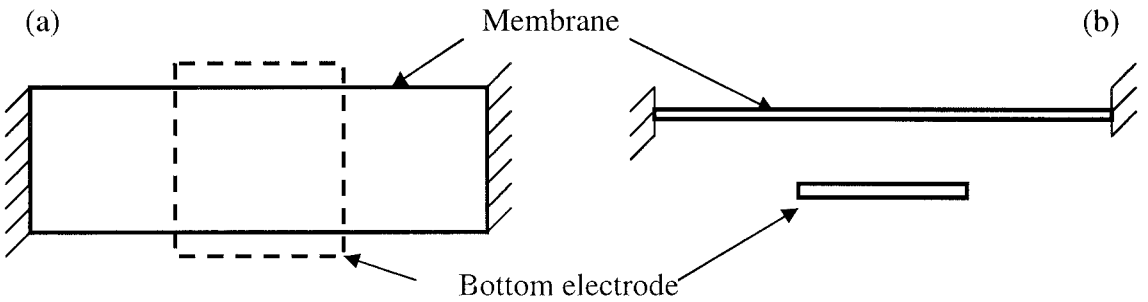

Figure 3. Schematic of the MEMS switch examined in this article: (a) top view; (b) cross-sectional view. Membrane length: 320 μm; membrane width: 110 μm; membrane thickness: 300 nm; bottom electrode length: 90 μm; bottom electrode width: 120 μm; gap between membrane and bottom electrode: 4 μm. There is a 200-nm-thick dielectric layer on top of the bottom electrode.

tion is not achievable. This corresponds to the unstable regime of the switch.

To illustrate the applicability of the FEA model discussed above, two corrugated membranes are examined along with a flat membrane. The schematic of the switches is shown in Figure 3. The membranes are rectangular with 320-μm length, 110-μm width, and 0.3-μm thickness. The length and width of the bottom electrode are 90 μm and 120 μm, respectively. The gap between the membrane and the bottom electrode is 4 μm, and the thickness of the dielectric layer on top of the bottom electrode is 0.2 μm. The switch membrane is made of aluminum and the substrate is silicon. The material properties for the switch membrane examined here are listed in Table 1. Two corrugated profiles used here are shown in Figures 4(a) and 4(b). Pressure is applied on the central part of the membrane on top of the bottom electrode. Figure 5(a) shows the pressure-deflection curves for flat membrane and the two corrugated membranes. It is seen that for the flat membrane, the 3rd-order nonlinear term is dominant [$\alpha = 3$ in eq. (3a)]; for the membrane with four corrugations, the linear term is more prominent; for the membrane with two corrugations, it is the combination of linear and nonlinear terms. It is seen that when the membrane is flat, the pressure-deflection curve is highly nonlinear. By contrast, corrugation linearizes the switch behavior. This result is well known and has been successfully used in the design of MEMS pressure sensors [25]. In the context of RF switches, this constitutive behavior affects the pull-in performance significantly, as shown in Figure

TABLE I. Membrane Material Properties [1]

Material Property	Value
Thermal expansion coefficient of Al (10^{-6}/K)	23.1
Thermal expansion coefficient of Si (10^{-6}/K)	2.6
Young's modulus of Al (GPa)	70
Poisson ratio of Al	0.35

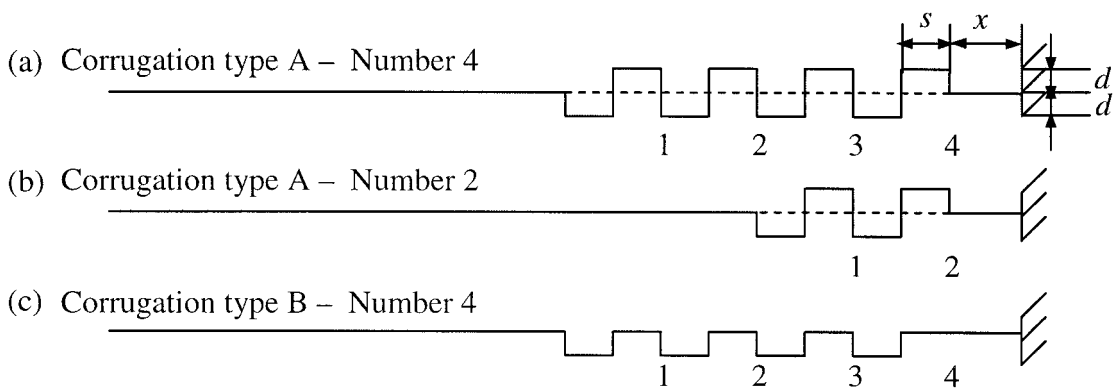

Figure 4. Several corrugated membranes and related geometric parameters: (a) corrugation type A with four corrugations; (b) corrugation type A with two corrugations; (c) corrugation type B with four corrugations. As labeled in (a), d denotes corrugation depth, s corrugation spacing, and x the distance away from the anchors. For corrugation type A, d is equal for both above and below the flat membrane; s is equal for both top and bottom parts.

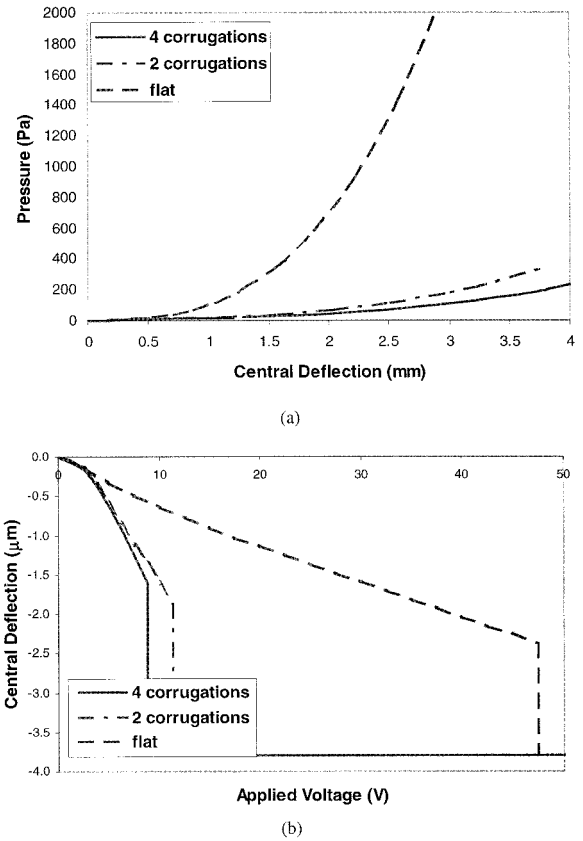

Figure 5. (a) Pressure-deflection curves and (b) pull-in curves for corrugation type A (four corrugations), corrugation type A (two corrugations), and flat membranes.

5(b). Note that the corrugation produces a major drop in pull-in voltage while preserving the in-plane geometry. This result is consistent with the prediction from 1D nonlinear model [Fig. 1 (a)]. This implies that a lumped model with a proper spring constant can describe a capacitive MEMS switch at large deflections accurately.

III. SWITCH RELIABILITY AS A FUNCTION OF TEMPERATURE

By employing the above FEA model, the effects of residual stress, out-of-plane membrane profile, and temperature were investigated [11]. For applications such as airplane condition monitoring and satellite wireless communication, the effect of low temperature was examined in detail. At these low temperatures, the pull-in voltage of a flat membrane becomes excessively high and beyond the reliable range. Two out-of-plane profiles were arbitrary selected in [11] to illustrate that, by tailoring the membrane structure, the pull-in voltage can be controlled within a certain range. However, these profiles are difficult to achieve in terms of micro-fabrication and are not necessarily optimal.

In this article, we investigate a more controllable profile—corrugated membrane—at both low and high temperatures. When a mismatch in thermal coefficient of expansion exists between substrate and membrane, high temperature leads to compressive stresses in the switch membrane, which may cause its buckling. To avoid this phenomenon, a residual tensile stress is required to balance the thermally induced compressive stress. During microfabrication, dry etching is used to etch the sacrificial layer under the switch membrane. When the sacrificial layer is etched away, the switch is then released and can move freely. This etching process takes place in a temperature up to 150°C. Therefore, the etch-release temperature of 150°C is used as the stress-free temperature in this study. Typically, a tensile stress develops in the membrane when the system is cooled down to room temperature. Note that in this article room temperature refers to 20°C. This is the case because the substrate has a much smaller thermal expansion coefficient than the typical materials used in the membranes, for example, Au or Al.

Basically, we examined two types of corrugations, corrugation types *A* and *B*, as shown in Figure 4. First, corrugation type B with four corrugations was examined. This type of corrugation has the advantage of ease of fabrication. However, when it was cooled down from 150°C to room temperature, the membrane buckled, which is undesirable.

Next, corrugation type A was examined with four and two corrugations, respectively [Figs. 4 (a) and (b)]. The effect of operational temperature on switch behavior is shown in Figures 6(a), 6(b), and 6(c) for membrane type A with four corrugations, with two corrugations, and no corrugations (flat), respectively. The temperature was varied from −60°C to 100°C. It was observed that in all cases a temperature reduction from room temperature increases the pull-in voltage, and a temperature increase reduces the pull-in voltage. The pull-in voltages for these three profiles, as a function of temperature, are summarized in Figure 7. In the above temperature range, the pull-in voltage varies from 25 to 45 V for four corrugations, from 32.5 to 62.5 V for two corrugations, and from 130 to 240 V for the flat membrane. The type-A membrane with four corrugations shows a promising behavior in preserving pull-in voltage within a reasonable range. It may be surprising to observe such large pull-in voltages for the flat membrane. However, a completely flat membrane is rarely achieved in practice. In fact, all capacitive MEMS switches have certain sur-

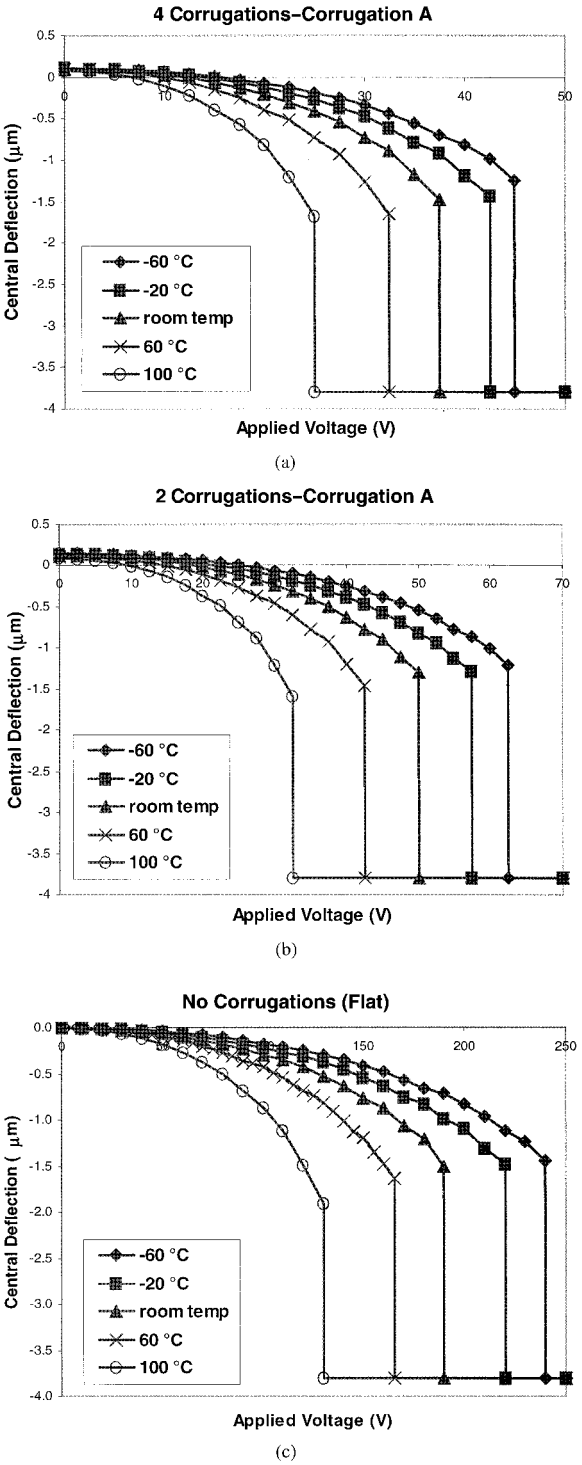

Figure 6. Central deflection-applied voltage curves for a rectangular switch with (a) type A (four corrugations), (b) type A (two corrugations), and (c) a flat membrane. Note that room temperature refers to 20°C.

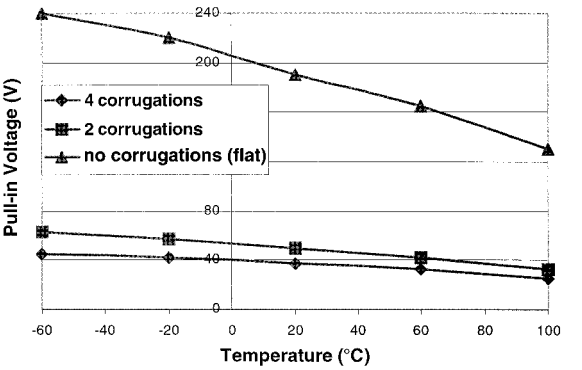

Figure 7. Pull-in voltages for three out-of-plane profiles: flat and corrugated type A with two and four corrugations, as a function of temperature.

face waviness that contributes to reduce the pull-in voltage considerably [14–16].

Temperature effects on pull-in voltage can be further understood by examining two device characteristics: membrane out-of-plane profile and resulting thermal stresses before actuation of the switch. For membrane type A with four corrugations, when cooled down from 150°C to room temperature, a tensile stress is induced and the corrugated profile changes correspondingly. Figure 8(a) shows the displacement contour in the *Z*-direction from 150°C to room temperature. Figure 8(b) is a magnified view of the initial corrugated profile and profile after the cooling along the center line of the switch. Due to symmetry, only half of the profiles are shown. During the cooling, the membrane displaces up by a small amount ($\sim$0.2 μm) and the corrugated profile remains nearly unchanged. This is due to the symmetric nature of the corrugation. By contrast, the corrugation type B buckles due to this temperature reduction. Note that the profile proposed in [11] is subjected to a downward displacement ($>$1 μm) and the profile changes quite dramatically. Figure 8(c) shows distribution of the Cauchy stress in the *X*-direction. Although very high-tensile and compressive stresses exist locally in the corrugated regions, the average stress in the central flat region is about 6.5 MPa.

The effects of the corrugation parameters are worthy of further investigation in order to guide optimal device design. These parameters include corrugation depth *d*, corrugation spacing *s*, and number of corrugations, as defined in Figure 4. The effects of these parameters are shown in Figure 9. Note that when these parameters are varied, the distance away from the edges (as defined in Fig. 4) remains constant. It is observed that with the increase of the corrugation depth, the pull-in voltages at both high and low tem-

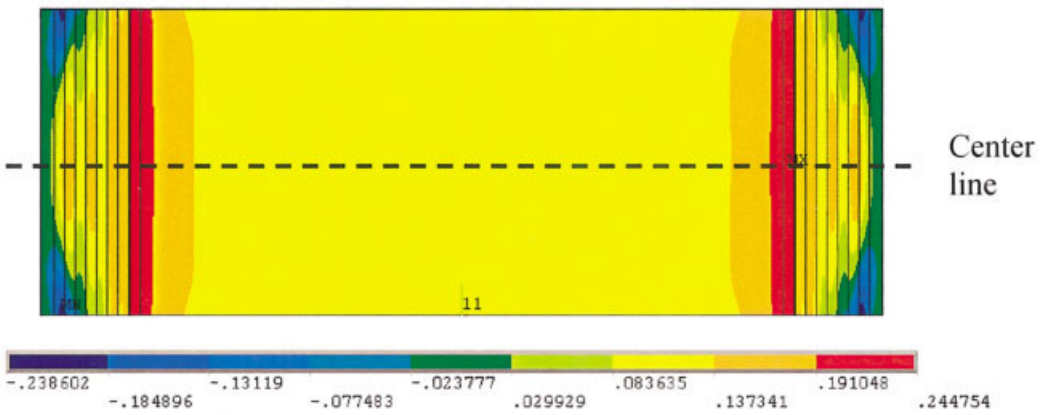

(a)

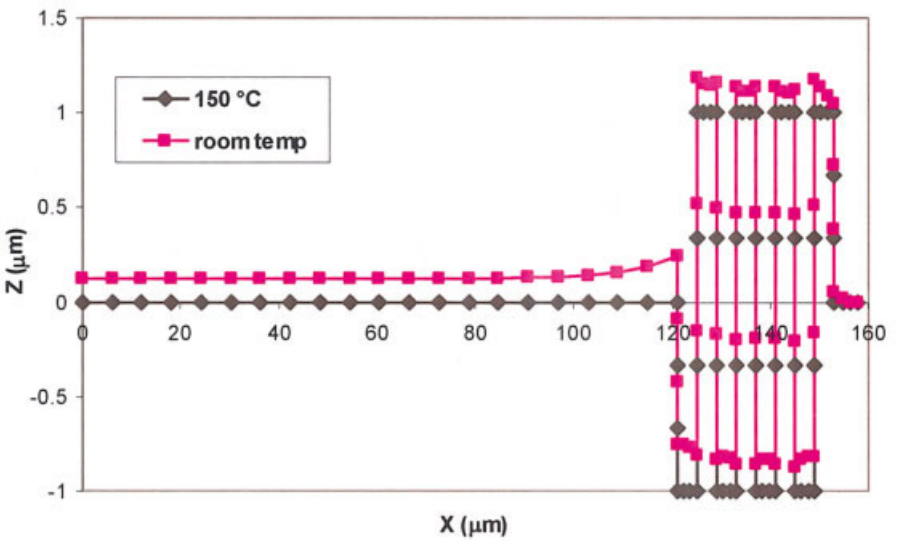

(b)

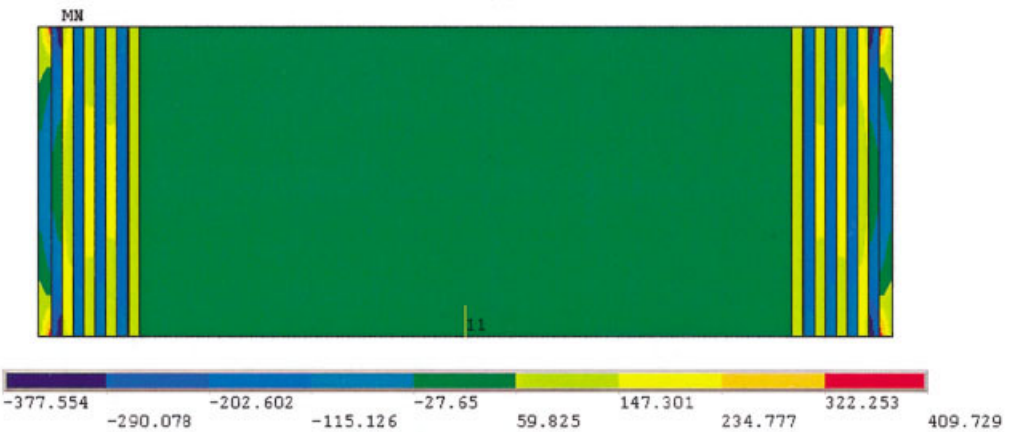

(c)

Figure 8. (a) *Z*-displacement contour of the type A membrane with four corrugations; (b) magnified *z*-displacement along the center line in (a) (only half is plotted due to symmetry); (c) Cauchy stress distribution in the *X*-direction (the average stress in the central flat region is 6.5 MPa). [Color figure can be viewed in the online issue, which is available at www.interscience.wiley.com.]

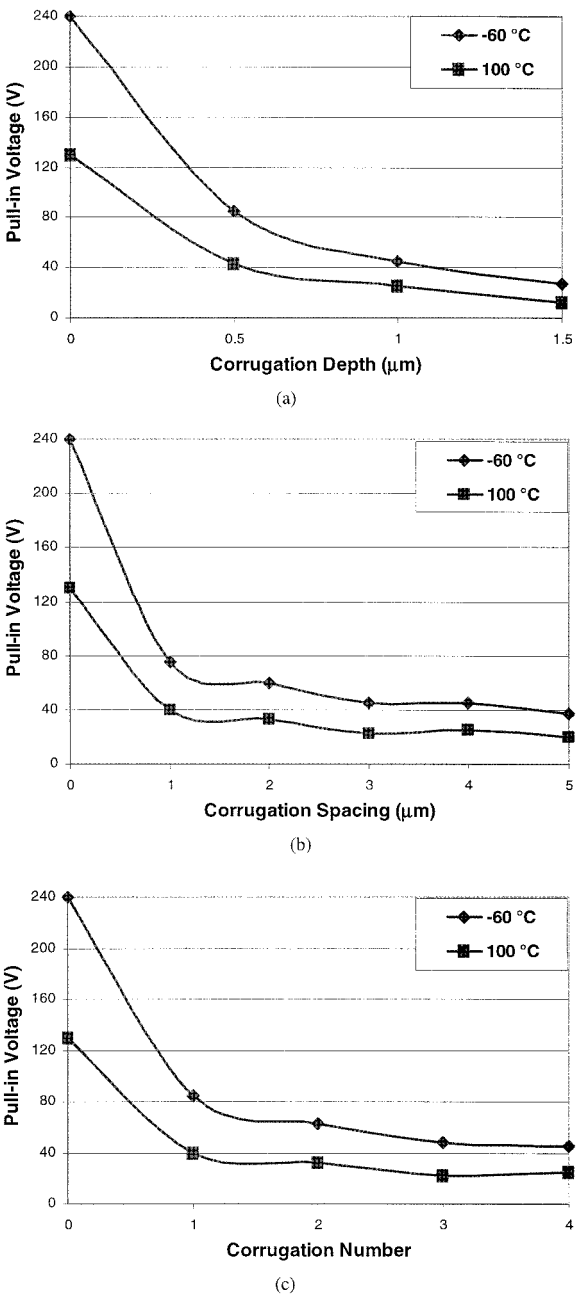

Figure 9. Effects of corrugation geometric parameters on the switch pull-in voltage: (a) corrugation depth; (b) corrugation spacing; (c) number of corrugations.

peratures are reduced considerably. From Figure 9(b) it is inferred that corrugation spacing in the range of 3–5 μm does not affect pull-in voltages for the examined temperature range. However, when the corrugation spacing is below 1 μm, the pull-in voltage increases at a high rate. In relation to the number of corrugations, Figure 9(c) shows that even when three corrugations result in a slightly smaller $V_{pull\text{-}in}$ than that of four corrugations, at 100°C, four corrugations are preferable because the pull-in voltage variation in the −60°C to 100°C temperature range is smaller. The reader should note that through proper selection of these parameters, the pull-in voltage variation could be kept within 20 V in the temperature range of −60°C to 100°C.

IV. ON-CHIP EXPERIMENTATION TECHNIQUES

MEMS switches are expected to be actuated a large number of cycles in wireless or other applications. Hence, problems associated to stiction, relaxation of residual stresses that control the device performance, or even material fatigue can be envisioned. Moreover, as illustrated in the previous section, operational temperatures also affect the device performance. While numerical models can be effectively employed to address some of these aspects, on-chip testing of device reliability at various temperatures is required. Furthermore, mechanical parameters such as material Young's modulus and elastic limit, residual stresses, and device shape must be identified experimentally. It is therefore essential to accurately characterize these parameters for the purpose of assessing reliability of MEMS switches.

There are several major established experimental techniques for mechanical characterization of thin films and MEMS materials: the bulge test, Nix and co-workers [17], the micro-tensile test, Sharpe et al. [18], the membrane-deflection experiment (MDE) developed by Espinosa et al. [19], the nanoindentation test, Nix et al. [20], and Oliver and Pharr [21]. However, these techniques require specially microfabricated specimens, which is not suitable for on-chip testing of MEMS switches. Two techniques overcome this limitation: one is electromechanical testing (for example, the M-test developed by Osterberg and Senturia [9]), and the other is pure mechanical testing (for example, the on-chip membrane deflection experiment developed by Espinosa et al. [16, 22]). In both techniques, a combined experimental–computational approach is required to identify Young's modulus and residual stress state. As discussed in [11, 16], accounting for the membrane out-of-plane profile is fundamental to the identification process.

In the M-test, a set of electrostatically actuated MEMS test structures is designed and fabricated. Pull-in voltages are measured using standard electronic measurement equipment in a MEMS probe station. Since the pull-in event is sudden and well defined, optical microscopy or RF circuitry can be

employed in its determination. Then, by using an analytical model that relates pull-in voltage of the test structure to material properties and residual stress state, these quantities can be identified (see Osterberg and Senturia [9]). Alternatively, following Chan et al. [23] capacitance-voltage (CV) measurements of fixed-fixed beams can be performed, and then material properties can be extracted with the aid of numerical simulations.

An alternative approach for on-chip device characterization is mechanical testing without the need of electromechanical actuation. This approach is well suited to complex device geometries including arbitrary out-of-plane geometries. Following Espinosa et al. [16, 22], a combined experimental–computational method can be employed to characterize material properties and residual stress state of RF MEMS. The overall experimental–computational approach consists of:

- device geometric characterization, i.e., measurement of dimensions and topography using full field optical profilometry;
- membrane deflection experiment (MDE), to interrogate the structural response of the device;
- 3D finite-element analysis (FEA), to reproduce the experimentally measured load-deflection curve by iterating Young's modulus, out-of-plane profile, and residual stress state.

Comparison between experiments and simulations provides a means to match load-deflection curves when an error norm is defined. In Figure 10, we reproduce the result reported by Espinosa et al. [16]. The switch membrane examined in such a study had certain out-of-plane waviness, especially close to the fixed ends. Their identification process resulted in a Young's modulus of 75 GPa and a nonuniform residual stress state, with a tensile stress of about 6 MPa in the relatively flat part of the membrane. By contrast, close to the edges, compressive stresses as high as 24 MPa were observed. Note that these findings were in agreement with the nonuniform stress distribution identified by Chen et al. [24], by employing a different methodology, for the same MEMS device.

While the M-test and MDE were developed for on-chip material characterization, its applicability to device reliability studies is straightforward. For instance, both types of tests can be performed at various temperatures although experimental difficulties need to be overcome. They can be used to identify in-plane membrane stress state as a function of temperature and its effect on $V_{pull\text{-}in}$. Furthermore, the electrostatic and mechanical testing could also be combined to examine the evolution of the device with actuation number. The device can be actuated and/or thermally cycled for a large number of cycles and then the MDE test can be used to identify the remaining residual stress field and overall structural stiffness. The combination of thermal, electrostatic, and mechanical loading offers many possibilities and advantages that still need to be explored.

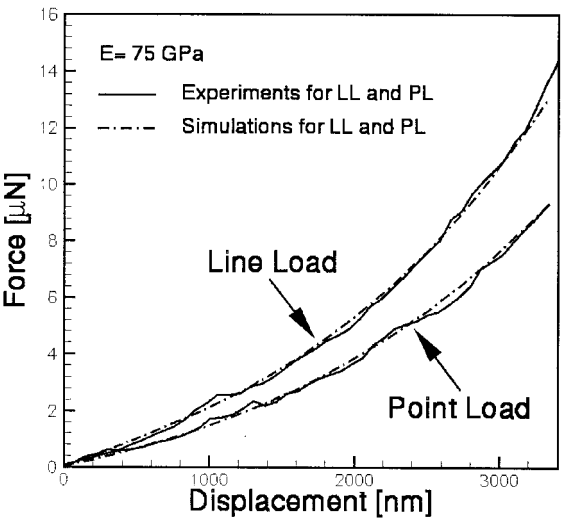

Figure 10. Comparison of numerical simulations with experiments of force-displacement curves for both line load and point load for $E = 75$ GPa and nonuniform residual stress. The identified residual stress in the relative flat region ranges is about 6 MPa [16].

V. CONCLUDING REMARKS

Due to some application requirements and the device packaging, there is an important need for understanding the impact of RF MEMS switch design on its performance as a function of temperature. High temperatures may cause buckling of the switch structure, which would lead to device failure. By contrast, low temperatures may result in an undesirably high pull-in voltage that can compromise the device life by charge build-up or lead to other failure modes.

This article has addressed this issue by discussing modeling and experimentation approaches and, in particular, by analyzing a promising stress-relaxation structure based on membrane corrugation. The major conclusions of the study are summarized as follows.

1D, 2D, and 3D models at both small deflections (linear) and large deflections (nonlinear) regimes are suitable to describe device behavior under certain conditions. Coupled-field 3D models are re-

quired to account for complex geometries and temperature histories. It is shown that linear and nonlinear models exhibit highly different device responses. The choice of model is a function of the objective of the analysis and desired accuracy. It is also shown that with a properly identified nonlinear spring, the 1D nonlinear lumped model can accurately describe the switch behavior at large deflections.

Out-of-plane membrane geometry is an important design variable. Depending on this feature, the switch may exhibit a highly nonlinear or linear response. It may be highly sensitive to temperature variations or approximately insensitive. In the later case, its reliable performance encompasses applications in which low or high temperatures are expected (for example, distributed satellite communication and aircraft condition monitoring).

The corrugated membrane exhibits a much advantageous performance over the flat membrane in the range $-60°C$ to $100°C$. In fact, corrugated membranes can be designed to be quite insensitive to temperature changes.

Corrugation geometric parameters (corrugation depth, corrugation spacing, and number of corrugations) are all features controlling the pull-in voltage sensitivity to temperature variations. Optimization algorithms can be combined with the analysis methodology discussed in this article in order to achieve optimal design.

Two types of on-chip experimental techniques, M-test and MDE, can be used in switch-reliability studies. These techniques can be also used in the on-chip characterization of mechanical properties, residual stress state, and device stiffness. An identification iterative process is required.

ACKNOWLEDGMENTS

The authors acknowledge support from the FAA through award no. DTFA03-01-C-00031 and the NSF through award no. CMS-0120866. We would like to express our appreciation to Drs. J. Newcomb and J. Larsen-Base for supporting this work.

REFERENCES:

1. G.M. Rebeiz, RF MEMS: Theory, design and technology, Wiley, New York, 2003.
2. C. Goldsmith, J. Ehmke, A. Malczewski, B. Pollans, S. Eschelman, Z. Yao, J. Brank, and M. Eberly, Life time characterization of capacitive RF MEMS switches, IEEE MTT-S Int Microwave Symp, Phoenix, AZ, 2001, pp. 227–230.
3. B.R. Norvell, R.J. Hancock, J.K. Smith, M.L. Pugh, S.W. Theis, and J. Kviatkofsky, Micro Electro Mechanical Switch (MEMS) technology applied to electronically scanned arrays for space based radar, IEEE Aerospace Conf, Aspen, CO 1999, pp. 239–247.
4. L.L. Mercado, T.Y.T. Lee, S.M. Kuo, and C. Amrine, Thermal solutions for discrete and wafer-level RF MEMS switch packages, IEEE Trans Adv Packaging 26 (2003), 318–326.
5. X. Lafontan, C. Le Touze, B. Wenk, I. Kolesnik, F. Pressecq, G. Perez, J.-M. Nicot, M. Dardalhon, and S. Rigo, Environmental test bench for reliability studies: influence of the temperature on RF switches with metallic membranes, Proc SPIE 4755 (2002), 624.
6. Z.J. Yao, S. Chen, S. Eshelman, D. Denniston, and C.L. Goldsmith, Micromachined low-loss microwavea switches, J Microelectromech Syst 8 (1999), 129–134.
7. C.L. Goldsmith, A. Malczewski, Z.J. Yao, S. Chen, J. Ehmke, and D.H. Hinzel, RF MEMS variable capacitors for tunable filters, Int J RF Microwave CAE 9 (1999), 362–374.
8. E.S. Hung and S.D. Senturia, Extending the travel range of analog-tuned electrostatic actuators, J Microelectromech Syst 8 (1999), 497–505.
9. P.M. Osterberg and S.D. Senturia, M-test: A test chip for MEMS material property measurement using electrostatically actuated test structures, J Microelectromech Syst 6 (1997), 107–118.
10. P.M. Osterberg, R.K. Gupta, J.R. Gilbert, and S.D. Senturia, Quantitative models for the measurement of residual stress, poisson's ratio, and Young's modulus using electrostatic pull-in of beams and diaphragms, Solid-State Sensor Actuator Wkshp, 1994, pp 184–188.
11. Y. Zhu and H.D. Espinosa, Effect of temperature on capacitive RF MEMS switch performance: A coupled-field analysis, J Micromech. Microengg (accepted).
12. Y. Zhu and H.D. Espinosa, Design of radio frequency (RF) MEMS switches: Modeling, Proc ASME Int Mech Eng Congress Exp, Washington, D.C., 2003.
13. P.L. Gould, Analysis of shells and plates, Springer-Verlag, New York, 1988.
14. X. Chauffleur, L. Rabbia, P. Pons, K. Grenier, R. Plana, and L. Dantas, Effect of membrane shape on mechanical behavior of RF switches, 16th Euro Conf Solid-State Transducers, Prague, Czech Republic, 2002, pp. 92–95.
15. G.-L. Tan and G.M. Rebeiz, A DC-contact MEMS shunt switch, IEEE Microwave Wireless Comp Lett 12 (2002), 212–214.
16. H.D. Espinosa, Y. Zhu, M. Fischer, and J. Hutchinson, An experimental/computational approach to identify moduli and residual stress in MEMS RF-switches, Experimental Mechanics 43 (2003), 309–316.
17. J. Vlassak and W. Nix, A new bulge test technique for the determination of Young's modulus and poi-

son's ratio of thin films, J Mat Res 7 (1992), 3242–3249.
18. B. Yuan and W. Sharpe, Jr., Mechanical testing of polysilicon thin films with the ISDG, Experimental Tech 21 (1997), 32–35.
19. H.D. Espinosa, B.C. Prorok, and M. Fischer, A methodology for determining mechanical properties of freestanding thin films and MEMS materials, J Mech Phys Solids 51 (2003), 47–67.
20. W. Nix, Elastic and plastic properties of thin films on substrates: nanoindentation techniques, Mat Sci Engg A, vol. 234–236 (1997), 37–44.
21. W.C. Oliver and G.M. Pharr, An improved technique for determining hardness and elastic-modulus using load and displacement sensing indentation experiments, J Mater Res.7 (1992), 1564–1583.
22. H.D. Espinosa, M. Fischer, Y. Zhu, and S. Lee, 3D computational modeling of RF MEMS switches, Proc 4th Int Conf Modeling Simulation Microsyst, Hilton Head Island, SC, 2001, pp. 402–405.
23. E.K. Chan, K. Garikipati, and R.W. Dutton, Characterization of contact electromechanics through capacitance-voltage measurements and simulations, J Microelectromech Syst 8 (1999), 208–217.
24. S. Chen, T.V. Baughn, Z.J. Yao, and C.L. Goldsmith, A new in-situ residual stress measurement method for a MEMS thin fixed-fixed beam structure, J Microelectromechan Syst 11 (2002), 309–316.
25. C.J. van Mullem, K.J. Gabriel, and H. Fujita, Large deflection performance of surface micromachined corrugated diaphragms, Proc Transducers '91, 1991, pp. 1014–1017.

BIOGRAPHIES

Yong Zhu received his Bachelor's degree from the University of Science and Technology of China in 1999. He received his Master's degree in mechanical engineering from Northwestern University in 2001. He is currently pursuing his Ph.D. degree in mechanical engineering at Northwestern University. His research interests include microelectromechanical systems (MEMS) design and testing, and micro- and nano-scale mechanical testing. As a graduate student, he was involved in reliability studies of RF MEMS switches. Since 2001, his research has focused on the design, fabrication, and testing of a MEMS-based test stage used for in-situ electron and atomic probe microscopy testing of nano-structures.

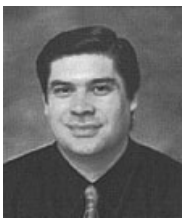

Horacio D. Espinosa is Associate Professor in the Department of Mechanical Engineering at Northwestern University. He received his degree in civil engineering from the Northeast National University, Argentina, in 1981, his M.Sc. in structural engineering from Politecnico di Milano, Italy, in 1987, and his M.Sc. in applied mathematics and Ph.D. in applied mechanics from Brown University, in 1991 and 1992, respectively. After receiving his Ph.D., he joined the Purdue University faculty and later moved to Northwestern University in 2000. He is the recipient of two young investigator awards, NSF-Career and ONR-YIP, and a Junior Award from the American Academy of Mechanics (AAM). He is also Fellow of the American Society of Mechanical Engineers (ASME) and AAM. He serves as Editor of *Mechanics*, a publication of the AAM and Associate Editor of the *Journal Experimental Mechanics*. His current research interests are on size-scale plasticity and fracture of thin films and MEMS/NEMS materials, in-situ electron and atomic probe microscopy testing of nanowires and CNTs, bio-inspired design of materials, and the development of MEMS devices for massively parallel atomic probe writing with chemicals and bio-molecules.